EUROPEAN ORGANIZATION FOR NUCLEAR RESEARCH

CERN-PPE/94-173
7 November 1994

A Study of $D^{*+}\pi^-$ Production in Semileptonic B Decay

The ALEPH Collaboration*

Abstract

In a sample of 1.5 million hadronic decays of the Z collected by the ALEPH detector, a search is carried out for the decays $\overline{\mathrm{B}} \to \mathrm{D}_1^0(2420)\ell^-\overline{\nu}\mathrm{X}$ and $\overline{\mathrm{B}} \to \mathrm{D}_2^{*0}(2460)\ell^-\overline{\nu}\mathrm{X}$. The product branching ratio for D_1^0 production is measured to be

$$\mathrm{Br}(\mathrm{b}\to \overline{\mathrm{B}}) \times \mathrm{Br}(\overline{\mathrm{B}} \to \mathrm{D}_1^0\ell^-\overline{\nu}\mathrm{X}) \times \mathrm{Br}(\mathrm{D}_1^0 \to \mathrm{D}^{*+}\pi^-) = (2.04 \pm 0.58_{\mathrm{stat}} \pm 0.34_{\mathrm{syst}}) \times 10^{-3},$$

and a 95% confidence level limit of

$$\mathrm{Br}(\mathrm{b}\to \overline{\mathrm{B}}) \times \mathrm{Br}(\overline{\mathrm{B}} \to \mathrm{D}_2^{*0}\ell^-\overline{\nu}\mathrm{X}) \times \mathrm{Br}(\mathrm{D}_2^{*0} \to \mathrm{D}^{*+}\pi^-) \leq 0.81 \times 10^{-3}$$

is obtained for D_2^{*0} production.
A topological search sensitive to the processes above, but also to wide resonances that decay to $\mathrm{D}^{*+}\pi^-$ and to non-resonant $\mathrm{D}^{*+}\pi^-$ production is also carried out, yielding

$$\mathrm{Br}(\mathrm{b}\to \overline{\mathrm{B}}) \times \mathrm{Br}(\overline{\mathrm{B}} \to \mathrm{D}^{*+}\pi^-\ell^-\overline{\nu}\mathrm{X}) = (3.7 \pm 1.0_{\mathrm{stat}} \pm 0.7_{\mathrm{syst}}) \times 10^{-3}.$$

Direct evidence of $\mathrm{D}^*\pi$ production inconsistent with D_1^0 and D_2^{*0} in semileptonic B decay is presented.

Submitted to Physics Letters B

* See following pages for the author list.

The ALEPH Collaboration

D. Buskulic, D. Casper, I. De Bonis, D. Decamp, P. Ghez, C. Goy, J.-P. Lees, M.-N. Minard, P. Odier, B. Pietrzyk

Laboratoire de Physique des Particules (LAPP), IN^{2}P^3-CNRS, 74019 Annecy-le-Vieux Cedex, France

F. Ariztizabal, M. Chmeissani, J.M. Crespo, I. Efthymiopoulos, E. Fernandez, M. Fernandez-Bosman, V. Gaitan, Ll. Garrido,[15] M. Martinez, S. Orteu, A. Pacheco, C. Padilla, F. Palla, A. Pascual, J.A. Perlas, F. Sanchez, F. Teubert

Institut de Fisica d'Altes Energies, Universitat Autonoma de Barcelona, 08193 Bellaterra (Barcelona), Spain[7]

D. Creanza, M. de Palma, A. Farilla, G. Iaselli, G. Maggi, N. Marinelli, S. Natali, S. Nuzzo, A. Ranieri, G. Raso, F. Romano, F. Ruggieri, G. Selvaggi, L. Silvestris, P. Tempesta, G. Zito

Dipartimento di Fisica, INFN Sezione di Bari, 70126 Bari, Italy

X. Huang, J. Lin, Q. Ouyang, T. Wang, Y. Xie, R. Xu, S. Xue, J. Zhang, L. Zhang, W. Zhao

Institute of High-Energy Physics, Academia Sinica, Beijing, The People's Republic of China[8]

G. Bonvicini, P. Comas, P. Coyle, H. Drevermann, A. Engelhardt, R.W. Forty, M. Frank, G. Ganis, C. Gay,[3] M. Girone, R. Hagelberg, J. Harvey, R. Jacobsen, B. Jost, J. Knobloch, I. Lehraus, M. Maggi, C. Markou, E.B. Martin, P. Mato, H. Meinhard, A. Minten, R. Miquel, P. Palazzi, J.R. Pater, P. Perrodo, J.-F. Pusztaszeri, F. Ranjard, L. Rolandi, D. Schlatter, M. Schmelling, W. Tejessy, I.R. Tomalin, R. Veenhof, A. Venturi, H. Wachsmuth, W. Wiedenmann, W. Witzeling, J. Wotschack

European Laboratory for Particle Physics (CERN), 1211 Geneva 23, Switzerland

Z. Ajaltouni, M. Bardadin-Otwinowska, A. Barres, C. Boyer, A. Falvard, P. Gay, C. Guicheney, P. Henrard, J. Jousset, B. Michel, S. Monteil, J-C. Montret, D. Pallin, P. Perret, F. Podlyski, J. Proriol, J.-M. Rossignol, F. Saadi

Laboratoire de Physique Corpusculaire, Université Blaise Pascal, IN^{2}P^3-CNRS, Clermont-Ferrand, 63177 Aubière, France

T. Fearnley, J.B. Hansen, J.D. Hansen, J.R. Hansen, P.H. Hansen, S.D. Johnson, R. Møllerud, B.S. Nilsson

Niels Bohr Institute, 2100 Copenhagen, Denmark[9]

A. Kyriakis, E. Simopoulou, I. Siotis, A. Vayaki, K. Zachariadou

Nuclear Research Center Demokritos (NRCD), Athens, Greece

A. Blondel, G. Bonneaud, J.C. Brient, P. Bourdon, L. Passalacqua, A. Rougé, M. Rumpf, R. Tanaka, A. Valassi, M. Verderi, H. Videau

Laboratoire de Physique Nucléaire et des Hautes Energies, Ecole Polytechnique, IN^{2}P^3-CNRS, 91128 Palaiseau Cedex, France

D.J. Candlin, M.I. Parsons, E. Veitch

Department of Physics, University of Edinburgh, Edinburgh EH9 3JZ, United Kingdom[10]

E. Focardi, G. Parrini

Dipartimento di Fisica, Università di Firenze, INFN Sezione di Firenze, 50125 Firenze, Italy

M. Corden, M. Delfino,[12] C. Georgiopoulos, D.E. Jaffe

Supercomputer Computations Research Institute, Florida State University, Tallahassee, FL 32306-4052, USA [13,14]

A. Antonelli, G. Bencivenni, G. Bologna,[4] F. Bossi, P. Campana, G. Capon, F. Cerutti, V. Chiarella, G. Felici, P. Laurelli, G. Mannocchi,[5] F. Murtas, G.P. Murtas, M. Pepe-Altarelli, S. Salomone

Laboratori Nazionali dell'INFN (LNF-INFN), 00044 Frascati, Italy

P. Colrain, I. ten Have,[6] I.G. Knowles, J.G. Lynch, W. Maitland, W.T. Morton, C. Raine, P. Reeves, J.M. Scarr, K. Smith, M.G. Smith, A.S. Thompson, S. Thorn, R.M. Turnbull

Department of Physics and Astronomy, University of Glasgow, Glasgow G12 8QQ,United Kingdom[10]

U. Becker, O. Braun, C. Geweniger, G. Graefe, P. Hanke, V. Hepp, E.E. Kluge, A. Putzer, B. Rensch, M. Schmidt, J. Sommer, H. Stenzel, K. Tittel, M. Wunsch

Institut für Hochenergiephysik, Universität Heidelberg, 69120 Heidelberg, Fed. Rep. of Germany[16]

R. Beuselinck, D.M. Binnie, W. Cameron, M. Cattaneo, D.J. Colling, P.J. Dornan, J.F. Hassard, N. Konstantinidis, L. Moneta, A. Moutoussi, J. Nash, D.G. Payne, G. San Martin, J.K. Sedgbeer, A.G. Wright

Department of Physics, Imperial College, London SW7 2BZ, United Kingdom[10]

G. Dissertori, P. Girtler, E. Kneringer, D. Kuhn, G. Rudolph

Institut für Experimentalphysik, Universität Innsbruck, 6020 Innsbruck, Austria[18]

C.K. Bowdery, T.J. Brodbeck, A.J. Finch, F. Foster, G. Hughes, D. Jackson, N.R. Keemer, M. Nuttall, A. Patel, T. Sloan, S.W. Snow, E.P. Whelan

Department of Physics, University of Lancaster, Lancaster LA1 4YB, United Kingdom[10]

A. Galla, A.M. Greene, K. Kleinknecht, J. Raab, B. Renk, H.-G. Sander, H. Schmidt, S.M. Walther, R. Wanke, B. Wolf

Institut für Physik, Universität Mainz, 55099 Mainz, Fed. Rep. of Germany[16]

A.M. Bencheikh, C. Benchouk, A. Bonissent, D. Calvet, J. Carr, C. Diaconu, F. Etienne, D. Nicod, P. Payre, L. Roos, D. Rousseau, M. Talby

Centre de Physique des Particules, Faculté des Sciences de Luminy, IN^{2}P^3-CNRS, 13288 Marseille, France

I. Abt, S. Adlung, R. Assmann, C. Bauer, W. Blum, D. Brown, P. Cattaneo,[23] B. Dehning, H. Dietl, F. Dydak,[21] A.W. Halley, K. Jakobs, H. Kroha, J. Lauber, G. Lütjens, G. Lutz, W. Männer, H.-G. Moser, R. Richter, J. Schröder, A.S. Schwarz, R. Settles, H. Seywerd, U. Stierlin,[2] U. Stiegler, R. St. Denis, G. Wolf

Max-Planck-Institut für Physik, Werner-Heisenberg-Institut, 80805 München, Fed. Rep. of Germany[16]

R. Alemany, J. Boucrot, O. Callot, A. Cordier, F. Courault, M. Davier, L. Duflot, J.-F. Grivaz, Ph. Heusse, M. Jacquet, P. Janot, D.W. Kim,[19] F. Le Diberder, J. Lefrançois, A.-M. Lutz, G. Musolino, I. Nikolic, H.J. Park, I.C. Park, M.-H. Schune, S. Simion, J.-J. Veillet, I. Videau

Laboratoire de l'Accélérateur Linéaire, Université de Paris-Sud, IN^{2}P^3-CNRS, 91405 Orsay Cedex, France

D. Abbaneo, G. Bagliesi, G. Batignani, S. Bettarini, U. Bottigli, C. Bozzi, G. Calderini, M. Carpinelli, M.A. Ciocci, V. Ciulli, R. Dell'Orso, I. Ferrante, F. Fidecaro, L. Foà,[1] F. Forti, A. Giassi, M.A. Giorgi, A. Gregorio, F. Ligabue, A. Lusiani, P.S. Marrocchesi, A. Messineo, G. Rizzo, G. Sanguinetti, A. Sciabà, P. Spagnolo, J. Steinberger, R. Tenchini, G. Tonelli,[26] G. Triggiani, C. Vannini, P.G. Verdini, J. Walsh

Dipartimento di Fisica dell'Università, INFN Sezione di Pisa, e Scuola Normale Superiore, 56010 Pisa, Italy

A.P. Betteridge, G.A. Blair, L.M. Bryant, Y. Gao, M.G. Green, D.L. Johnson, T. Medcalf, Ll.M. Mir, J.A. Strong

Department of Physics, Royal Holloway & Bedford New College, University of London, Surrey TW20 OEX, United Kingdom[10]

V. Bertin, D.R. Botterill, R.W. Clifft, T.R. Edgecock, S. Haywood, M. Edwards, P. Maley, P.R. Norton, J.C. Thompson

Particle Physics Dept., Rutherford Appleton Laboratory, Chilton, Didcot, Oxon OX11 OQX, United Kingdom[10]

B. Bloch-Devaux, P. Colas, H. Duarte, S. Emery, W. Kozanecki, E. Lançon, M.C. Lemaire, E. Locci, B. Marx, P. Perez, J. Rander, J.-F. Renardy, A. Rosowsky, A. Roussarie, J.-P. Schuller, J. Schwindling, D. Si Mohand, A. Trabelsi, B. Vallage

CEA, DAPNIA/Service de Physique des Particules, CE-Saclay, 91191 Gif-sur-Yvette Cedex, France[17]

R.P. Johnson, A.M. Litke, G. Taylor, J. Wear

Institute for Particle Physics, University of California at Santa Cruz, Santa Cruz, CA 95064, USA[22]

A. Beddall, C.N. Booth, C. Boswell, S. Cartwright, F. Combley, I. Dawson, A. Koksal, M. Letho, W.M. Newton, C. Rankin, L.F. Thompson

Department of Physics, University of Sheffield, Sheffield S3 7RH, United Kingdom[10]

A. Böhrer, S. Brandt, G. Cowan, E. Feigl, C. Grupen, G. Lutters, J. Minguet-Rodriguez, F. Rivera,[25] P. Saraiva, U. Schäfer, L. Smolik

Fachbereich Physik, Universität Siegen, 57068 Siegen, Fed. Rep. of Germany[16]

L. Bosisio, R. Della Marina, G. Giannini, B. Gobbo, L. Pitis, F. Ragusa[20]

Dipartimento di Fisica, Università di Trieste e INFN Sezione di Trieste, 34127 Trieste, Italy

H. Kim, J. Rothberg, S. Wasserbaech

Experimental Elementary Particle Physics, University of Washington, WA 98195 Seattle, U.S.A.

S.R. Armstrong, L. Bellantoni, J.S. Conway,[24] P. Elmer, Z. Feng, D.P.S. Ferguson, Y.S. Gao, S. Gonzáles, J. Grahl, J.L. Harton, O.J. Hayes, H. Hu, P.A. McNamara III, J.M. Nachtman, W. Orejudos, Y.B. Pan, Y. Saadi, M. Schmitt, I. Scott, V. Sharma, J.D. Turk, A.M. Walsh, F.V. Weber,[1] T. Wildish, Sau Lan Wu, X. Wu, J.M. Yamartino, M. Zheng, G. Zobernig

Department of Physics, University of Wisconsin, Madison, WI 53706, USA[11]

[1] Now at CERN, 1211 Geneva 23, Switzerland.
[2] Deceased.
[3] Now at Harvard University, Cambridge, MA 02138, U.S.A.
[4] Also Istituto di Fisica Generale, Università di Torino, Torino, Italy.
[5] Also Istituto di Cosmo-Geofisica del C.N.R., Torino, Italy.
[6] Now at TSM Business School, Enschede, The Netherlands.
[7] Supported by CICYT, Spain.
[8] Supported by the National Science Foundation of China.
[9] Supported by the Danish Natural Science Research Council.
[10] Supported by the UK Science and Engineering Research Council.
[11] Supported by the US Department of Energy, contract DE-AC02-76ER00881.
[12] On leave from Universitat Autonoma de Barcelona, Barcelona, Spain.
[13] Supported by the US Department of Energy, contract DE-FG05-92ER40742.
[14] Supported by the US Department of Energy, contract DE-FC05-85ER250000.
[15] Permanent address: Universitat de Barcelona, 08208 Barcelona, Spain.
[16] Supported by the Bundesministerium für Forschung und Technologie, Fed. Rep. of Germany.
[17] Supported by the Direction des Sciences de la Matière, C.E.A.
[18] Supported by Fonds zur Förderung der wissenschaftlichen Forschung, Austria.
[19] Permanent address: Kangnung National University, Kangnung, Korea.
[20] Now at Dipartimento di Fisica, Università di Milano, Milano, Italy.
[21] Also at CERN, 1211 Geneva 23, Switzerland.
[22] Supported by the US Department of Energy, grant DE-FG03-92ER40689.
[23] Now at Università di Pavia, Pavia, Italy.
[24] Now at Rutgers University, Piscataway, NJ 08854, USA.
[25] Partially supported by Colciencias, Colombia.
[26] Also at Istituto di Matematica e Fisica, Università di Sassari, Sassari, Italy.

1 Introduction

The composition of the inclusive semileptonic branching ratio of the B meson in terms of exclusive branching ratios is a long-standing problem which affects a number of studies. Experimentally, 39±6% of the inclusive rate is not accounted for [1] by the decays $\overline{\mathrm{B}} \to \mathrm{D}\ell^-\overline{\nu}$ and $\overline{\mathrm{B}} \to \mathrm{D}^*\ell^-\overline{\nu}$, contrary to initial expectations [2, 3, 4].

Two possible explanations are direct four-body decays, such as $\overline{\mathrm{B}} \to \mathrm{D}^*\pi\ell^-\overline{\nu}$, and decays to L=1 charm mesons. Four such mesons, with the properties listed in Table 1, are expected [5, 6, 7]. From Heavy Quark Effective Theory [8], the spin of the light quark combined with the angular momentum due to the orbital excitation, J_{lq}, is a conserved quantity in the limit of infinite heavy quark mass. States with J_{lq} of 3/2 are expected to be easily visible narrow resonances and two physical states, $\mathrm{D}_1(2420)$ and $\mathrm{D}_2^*(2460)$, have been observed [9] in two body decays. States with J_{lq} of 1/2 are expected to be wide resonances which cannot be distinguished from four-body decays with the available experimental statistics. This paper uses the term "non-resonant" to indicate both direct four-body decays and wide resonances.

	J^P	J_{lq}	Mass (MeV)	Width (MeV)	Decay Modes
	1^+	1/2	$\sim$ 2420 (unobserved)	$\gtrsim$250	$\mathrm{D}^*\ \pi$
	0^+	1/2	$\sim$ 2360 (unobserved)	$\gtrsim$170	$\mathrm{D}\ \pi$
D_1	1^+	3/2	2421±2	20±4	$\mathrm{D}^*\ \pi$
D_2^*	2^+	3/2	2458±2	23±6	$\mathrm{D}\ \pi$, $\mathrm{D}^*\pi$

Table 1: Charm mesons with orbital excitations, their quantum numbers, masses, widths, and allowed strong decays to D π and D$^*\pi$ in the infinite heavy quark mass limit.

The decay of the Z boson at LEP provides a source of boosted B mesons, and the tracking resolution of the ALEPH detector permits the identification of B meson decays using their distinctive vertex topology. Semileptonic decays of B mesons are reconstructed by identifying events containing a lepton[1] and a D^{*+}. The typical decay length of the B meson is 2.6mm, and can be measured with an average resolution of 280 μm. This is used to differentiate tracks originating at the B decay point from tracks originating at the primary interaction point.

This letter reports the measurements of the decays $\overline{\mathrm{B}} \to \mathrm{D}_1^0\ell^-\overline{\nu}\mathrm{X}$, $\overline{\mathrm{B}} \to \mathrm{D}_2^{*0}\ell^-\overline{\nu}\mathrm{X}$ and non-resonant $\overline{\mathrm{B}} \to \mathrm{D}^{*+}\pi^-\ell^-\overline{\nu}\mathrm{X}$ with the ALEPH detector at LEP. The data sample is 1.5 $\times 10^6$ hadronic decays of the Z collected in 1991, 1992, and 1993.

2 The ALEPH Detector

The ALEPH detector is described in detail in Reference [10], and only a brief description of the apparatus is given here.

A high resolution vertex detector (VDET) [11], consisting of two layers of double sided silicon microstrip detectors surrounds the beam pipe. The inner layer is at an average radius of 6.3 cm from the beam axis and covers 85% of the solid angle, and the outer layer is at an average radius of 10.8 cm and covers 69%. The spatial resolution for the $r\phi$ coordinate is 12 μm. For the z coordinate, it varies between 12 and 22 μm, depending on the polar angle of the track. The vertex detector is surrounded by a drift chamber (ITC) with eight axial wire layers up to a radius of 26 cm, and a time projection chamber (TPC) that measures up to 21 three-dimensional points per track at radii between 40 and 171 cm. These detectors are immersed in an axial magnetic field of 1.5 T and together provide a transverse momentum resolution of $\Delta p/p = 0.0006p$ (p in GeV/c), as measured with 45 GeV/c muons. For tracks with hits in both layers of the VDET, the resolution of

[1] In this paper, "leptons" will refer to either electrons or muons. Charge conjugate reactions are always implied.

the 3D impact parameter is $\sigma = 25\,\mu\mathrm{m} + 95\mu\mathrm{m}/p$ (p in GeV/c), in both the $r\phi$ and rz views. The TPC also provides up to 338 measurements of specific ionization of a track. It is surrounded by an electromagnetic calorimeter (ECAL) of lead / proportional-chamber construction, segmented into 15 mrad $\times$ 15 mrad projective towers and read out in three sections in depth, with energy resolution $\Delta(E)/E = 0.18/\sqrt{E}(E\,\mathrm{in\,GeV})$. The iron return yoke of the magnet is instrumented with streamer tubes to form a hadron calorimeter (HCAL), with a thickness of over 7 interaction lengths and it is surrounded by two additional double layers of streamer tubes to aid muon identification.

The interaction point is reconstructed on an event-by-event basis [12, 13], with a measured resolution of 85 μm, averaged over all directions for $b\overline{b}$ events.

3 $\overline{\mathrm{B}} \to \mathrm{D}_1^0 \ell^- \overline{\nu} \mathrm{X}$ and $\overline{\mathrm{B}} \to \mathrm{D}_2^{0*} \ell^- \overline{\nu} \mathrm{X}$

The decays $\overline{\mathrm{B}} \to \mathrm{D}_1^0 \ell^- \overline{\nu} \mathrm{X}$ and $\overline{\mathrm{B}} \to \mathrm{D}_2^{*0} \ell^- \overline{\nu} \mathrm{X}$ have a distinctive three vertex topology. For example, the decay

$$\begin{array}{l} \mathrm{B}^- \longrightarrow \mathrm{D}_1^0 \mu^- \overline{\nu} \\ \qquad \hookrightarrow \mathrm{D}^{*+}\ \pi_{**}^- \\ \qquad\quad \hookrightarrow \mathrm{D}^0\ \pi_*^+ \\ \qquad\qquad \hookrightarrow \mathrm{K}^-\pi^+ \end{array}$$

where π_*^+ denotes the pion from D^{*+} decay, and π_{**}^- denotes the pion from D_1^0 decay[2], has the topology shown in Fig. 1.

The primary background is from the decay $\overline{\mathrm{B}}^0 \to \mathrm{D}^{*+}\ell^-\overline{\nu}$, where a fragmentation track is poorly measured and assigned to the $\mathrm{D}^{*+}\ell^-$ vertex. Unlike the signal, it will produce π_{**} candidates of either sign. However, the combinations where the π_{**} is of the same sign as the lepton (*i.e.* the right sign) occur more often than the opposite (wrong) sign combinations, because the mean expected charge of the event hemisphere containing the $\mathrm{D}^{*+}\ell^-$ is non-zero.

The decays $\overline{\mathrm{B}} \to \mathrm{D}_1^0 \ell^- \overline{\nu} \mathrm{X}$ and $\overline{\mathrm{B}} \to \mathrm{D}_2^{*0} \ell^- \overline{\nu} \mathrm{X}$ are identified in events where a D^{*+} and a high momentum ($\geq 3\,\mathrm{GeV/c}$) lepton are found in the same hemisphere of a hadronic Z decay [14]. Electrons are identified by comparing the momentum measured in the TPC with the energy measured in the ECAL, the depth and shape of the ECAL shower, and the specific ionization information from the TPC. Including the momentum requirement, the electron identification efficiency is 62%, with a hadron misidentification rate of 2×10^{-3}. Muon candidates are accepted if they have a hit pattern characteristic of a penetrating particle in the HCAL or if they have at least two associated hits in the muon chambers. The muon identification efficiency is 66%, with a hadron misidentification rate of 8×10^{-3}. Lepton identification in ALEPH is described in detail in Reference [15] [3].

Two complementary approaches to event selection are taken. In one approach (Selection A), a large sample of $\mathrm{D}^{*+}\ell^-$ events is chosen, and stringent requirements are applied to ensure that the π_{**}^- candidate does not pass through the interaction point. In the second (Selection B), a cleaner sample of $\mathrm{D}^{*+}\ell^-$ events is chosen, and stringent requirements are then made on the quality of the $\mathrm{D}^{*+}\ell^-$ vertex and on the measurement of the π_{**}^- position relative to that vertex, but the requirement that the π_{**}^- candidate does not pass through the interaction point is relaxed. The overall efficiencies of the two selections are comparable.

3.1 Event Selection A

The D^{*+} is reconstructed in the channel $\mathrm{D}^{*+} \to \mathrm{D}^0\pi_*^+$, and the D^0 is reconstructed in four decay channels: $\mathrm{D}^0 \to \mathrm{K}^-\pi^+$, $\mathrm{D}^0 \to \mathrm{K}^-\pi^+\pi^-\pi^+$, $\mathrm{D}^0 \to \mathrm{K}^0_\mathrm{S}\pi^+\pi^-$, $\mathrm{D}^0 \to \mathrm{K}^-\pi^+\pi^0$. The mass differ-

[2] The symbol π_{**}^- also denotes pions from non-resonant decays.

[3] For this paper, the requirement that $\mathrm{d}E/\mathrm{d}x$ information be available for electron candidates was dropped, and muon candidates with hits in both layers of the muon chambers passing tight matching criteria were also accepted.

ence $m(D^0\pi^+_*)-m(D^0)$ is required to be within two standard deviations ($\sigma \sim 0.75\,\mathrm{MeV/c^2}$) of $145.5\,\mathrm{MeV/c^2}$. The electron momentum cut is lowered to 2 GeV/c to increase the acceptance for the $D^{*+}\ell^-$ sample. The vertex formed by the D^0 decay products is required to be separated from the interaction point by more than twice the resolution of the decay distance for that event, and the reconstructed mass must lie within two sigma of the known D^0 mass. The D^0 mass resolution in the different decay channels is given in Table 2. For channels with a charged kaon, the specific ionization measurement, when available, must be consistent (within two sigma) with the expected rate for kaons. For $D^0 \to K^-\pi^+\pi^-\pi^+$ and $D^0 \to K^0_S\,\pi^+\pi^-$, the momentum of the kaon is required to be over 2.0 GeV/c. For $D^0 \to K^-\pi^+\pi^0$, the momentum of the K^- is required to be larger than 3.0 GeV/c, and the momentum of both pions to be more than 1.5 GeV/c. In the $K^-\pi^+\pi^-\pi^+$ channel, the D^0 candidate is rejected if the fit of the four tracks to a common vertex has a χ^2 probability of less than 0.1%. Candidate K^0_S are rejected if the decay length is less than 2.0 cm or if the measured mass is more than two standard deviations ($\sigma \sim 5\,\mathrm{MeV/c^2}$) from the K^0_S mass. Neutral pions are identified by fitting pairs of ECAL energy deposits using the constraint that the mass of the pair is the π^0 mass. Candidate π^0 are rejected if the χ^2 of this fit corresponds to a probability of less than 1.0%. Table 2 lists the D^{*+} candidate subsample sizes and background rates as estimated from a fit to the sidebands for both selections.

To identify pions from D^0_1 and D^{*0}_2 decay, a momentum requirement is used, since these pions have a harder momentum spectrum than fragmentation tracks. This requirement on the momentum of the π^-_{**} candidate also reduces multiple scattering uncertainties. The π^-_{**} candidate is therefore required to have a momentum greater than 1 GeV/c. To further reduce tracking uncertainties, the π^-_{**} is required to have at least one VDET hit. To reject fragmentation tracks, the impact parameter of the π^-_{**} relative to the interaction point is required to be more than three times its uncertainty. The χ^2 of the $D^{*+}\ell^-\pi^-_{**}$ vertex is required to correspond to a probability of 1% or better. The efficiencies are given in Table 3.

3.2 Event Selection B

The D^{*+} is also reconstructed in the channel $D^{*+} \to D^0\pi^+$, and the D^0 is reconstructed in the decay modes $D^0 \to K^-\pi^+$ and $D^0 \to K^-\pi^+\pi^-\pi^+$. The procedure is described in more detail in Reference [16].

The D^0 candidate is required to have a momentum greater than 7 GeV/c. In the channel $D^0 \to K^-\pi^+\pi^-\pi^+$, the specific ionization measurement, when available, must be consistent (within two sigma) with the expected rate for kaons. In addition, the momentum of at least two of the four D^0 decay tracks is required to be greater than 1 GeV/c.

The χ^2 of the $D^{*+}\ell^-$ vertex fit is required to be less than 5 for 3 d.o.f., corresponding to a probability of 17.2%. The calculated uncertainty on the B decay length is required to be less than 500 μm, and a $D^{*+}\ell^-$ candidate is rejected if the distance of the vertex from the interaction point is less than twice the uncertainty. Furthermore, the $D^{*+}\ell^-$ vertex is required to be upstream of the D^0 vertex. Finally, the invariant mass of the $D^{*+}\ell^-$ system must lie between 2.7 and $4.5\,\mathrm{GeV/c^2}$. Table 2 lists the D^{*+} candidate subsample sizes, background rates as estimated from a fit to the sidebands for both selections, and the D^0 mass resolutions.

If the impact parameter of a candidate π^-_{**} relative to the interaction point is less than its uncertainty, the candidate is rejected. The error on the impact parameter relative to the $D^{*+}\ell^-$ vertex is required to be less than 250 μm. The impact parameter of the π^-_{**} with respect to the $D^{*+}\ell^-$ vertex divided by its resolution, δ/σ_δ, is shown for simulated signal events in Fig. 2(a), for background events in Fig. 2(b), and for the data in Fig. 2(c). The distribution for signal events is fitted to $A_1(x\exp -x^2/2\sigma^2) + A_2(x\exp -x/\lambda)$, where the second term is included to model the tail due to non-Gaussian effects in the tracking. The fit to δ/σ_δ is used to calculate the probability Π that the π^-_{**} originates from the $D^{*+}\ell^-$ vertex:

$$\Pi = \int_{\delta/\sigma_\delta}^{\infty} R_\delta(x)dx. \qquad (1)$$

where $R_\delta(\delta/\sigma_\delta)$ is the fitted function. The π^-_{**} is required to have a probability of originating from the $D^{*+}\ell^-$ vertex greater than 10%. The efficiencies are given in Table 3.

Channel	D^0 resolution (MeV/c^2)	Selection A		Selection B	
		$D^{*+}\ell^-$	bkg.	$D^{*+}\ell^-$	bkg.
$D^0 \to K^-\pi^+$	12	322±20	30±5	133±17	1.7±0.7
$D^0 \to K^-\pi^+\pi^-\pi^+$	9	341±21	72±3	179±14	20.5±2.3
$D^0 \to K^0_S\pi^+\pi^-$	10	97±10	18±2	—	—
$D^0 \to K^-\pi^+\pi^0$	23	226±20	116±7	—	—

Table 2: D^0 mass resolutions, fitted number of $D^{*+}\ell^-$ and background events within a $\pm 2\sigma$ window around the fitted mass.

Channel	Selection A Signal Efficiency	Selection B Signal Efficiency
$D^0 \to K^-\pi^+$	8.41±1.16%	7.93±1.42%
$D^0 \to K^-\pi^+\pi^-\pi^+$	3.38±0.54%	5.88±0.90%
$D^0 \to K^0_S\pi^+\pi^-$	3.27±0.56%	—
$D^0 \to K^-\pi^+\pi^0$	1.10±0.19%	—

Table 3: Efficiencies for $\overline{B} \to D^0_1\ell^-\overline{\nu}$ for the four decay modes.

3.3 Results

The parameter Δm^{**} is defined as the difference between the measured masses of the $D^{*+}\pi^-_{**}$ system and the D^{*+}, and has a measurement error of 3 to 4 MeV/c^2, much less than the widths of the D^0_1 and D^{*0}_2 resonances. The distribution of Δm^{**}, as found in the data with event selections A and B are shown in Figs. 3 and 4, respectively.

The right sign distribution is first fit to two Breit-Wigner resonances with masses and widths set to the known values, plus a background function. In neither selection is there a significant contribution from D^{*0}_2. Accordingly, the quoted results are from a refit of the distribution retaining only the D^0_1 contribution.

There are $12.6 \pm^{5.0}_{4.2}$ events in the signal peak with selection A, and 16.8±5.0 with selection B. If the mass and width of the D^0_1 resonance are not constrained, the fitted mass and width of the resonance are respectively $2410 \pm^{6}_{7}$ MeV/c^2 and $33 \pm^{30}_{29}$ MeV/c^2 for event selection A, and 2424±4 MeV/c^2 and 20±3 MeV/c^2 respectively for event selection B.

The results from the two selection procedures are consistent. The complementarity of the two approaches to event selection results in event samples with little overlap. In the region of the resonance, only six events are found in common by both selection procedures, corresponding to a correlation coefficient of 41%. The results from the two selections are combined [17] to reduce the statistical and the uncorrelated systematic uncertainties. From the number of events in the resonant peak and the detection efficiency, the product branching ratio

$$\mathrm{Br}(b \to \overline{B}) \times \mathrm{Br}(\overline{B} \to D^0_1\ell^-\overline{\nu}X) \times \mathrm{Br}(D^0_1 \to D^{*+}\pi^-) = (2.04 \pm 0.58_{\mathrm{stat}} \pm 0.34_{\mathrm{syst}}) \times 10^{-3},$$

is measured.

To set a limit on the production of D^{*0}_2, the two distributions are refit, excluding the region within ±2 half-widths of the D^{*0}_2. These fits are used to estimate the background to any possible D^{*0}_2 contribution. Allowing for the overlap in the two selections, a 95% confidence level limit of 0.81×10^{-3} for the corresponding D^{*0}_2 product branching ratio is obtained.

3.4 Systematic Uncertainties

Most sources of systematic uncertainty are common to both selections. The mass and width of the D_1^0 resonance are varied by the uncertainties in their published values. The systematic uncertainty due to background subtraction is obtained by using several different parametrizations for the background function in the fit. The efficiency of the χ^2 requirement for the B decay vertex ($\sim 76\%$ for most channels) as calculated from Monte Carlo simulation is assigned a 10% uncertainty. The lepton identification efficiency is assigned an uncertainty of $\pm 5\%$. The momentum distributions of the decay products are primarily determined by the b fragmentation process in Z decay, and that is well measured from the study of inclusive lepton spectra [18]. There is a dependence of the efficiency on the lifetime of the B^- meson; the error is calculated by varying the lifetime by the uncertainty in its published value.

In event selection A, the entry for D^0 efficiencies includes the uncertainty in the correction to the efficiency calculated from Monte Carlo simulation for the vertex quality requirement in $D^0 \rightarrow K^-\pi^+\pi^-\pi^+$. An uncertainty of $\pm 10\%$ in the V^0 finding efficiency (which affects only the $K_S^0\,\pi^+\pi^-$ channel) is also included.

In event selection B, there is an uncertainty from the shape of the distribution of the distance from the $D^{*+}\ell^-$ to the π_{**}^-. This is estimated by varying the parameters of the fit to this distribution by their uncertainties.

The systematic uncertainties are summarized in Table 4.

Source	Selection A $\sigma_{syst}(10^{-3})$	Selection B $\sigma_{syst}(10^{-3})$
M,Γ of D_1^0	± 0.31	± 0.22
Background Function	± 0.25	± 0.15
B^- Vertex Efficiency	± 0.17	± 0.24
Monte Carlo Statistics	± 0.08	± 0.18
D^{*+}, D^0 Branching Ratios	± 0.06	± 0.10
Lepton ID Efficiency	± 0.09	± 0.12
b Fragmentation	± 0.03	± 0.03
B^- Lifetime	± 0.01	± 0.03
D^0 ID Efficiency	± 0.03	—
Probability Function Π	—	± 0.08
Total	± 0.45	± 0.44

Table 4: Systematic uncertainties for event selections A and B respectively, in $Br(b\rightarrow \overline{B}) \times Br(\overline{B} \rightarrow D_1^0 \ell^- \overline{\nu} X) \times Br(D_1^0 \rightarrow D^{*+}\pi^-)$.

4 $\overline{B} \rightarrow D^{*+}\pi_{**}^-\ell^-\overline{\nu}X$

In contrast to the previous cases, the resonant structure cannot be used to extract the signal in $\overline{B} \rightarrow D^{*+}\pi_{**}^-\ell^-\overline{\nu}X$. Nevertheless, the characteristic topology of this decay mode is sufficient for its identification.

4.1 Event Selection

The event selection begins with the clean $D^{*+}\ell^-$ sample of the selection B, and stringent requirements are then applied to the π_{**}^- candidates. The distance from the interaction point to the $D^{*+}\ell^-$ vertex is required to be greater than three times its uncertainty. The candidate π_{**}^- is accepted if the error on the distance from the $D^{*+}\ell^-$ vertex is less than 150 μm and if its impact parameter with respect to the interaction point is more than 2.5 times its measurement error. In

the $D^0 \to K^-\pi^+\pi^-\pi^+$ decay channel, the lower limit of the invariant mass of the $D^{*+}\ell^-$ system is increased to $3\,\mathrm{GeV/c^2}$.

If there is more than one π^-_{**} candidate, the one with the greatest momentum is chosen. This occurs for one event in $D^0 \to K^-\pi^+$ and for two events in $D^0 \to K^-\pi^+\pi^-\pi^+$.

4.2 Results

The probability distribution Π is described in Section 3.2. By construction it is uniform between zero and one for signal events. For background events it is peaked towards low values of Π, as shown in Fig. 5(a). The distribution of the signal probability in the data is shown in Fig. 5(b). There is a clear excess of 18 events with a high probability ($\Pi > 0.2$) in the right sign sample, and no corresponding excess in the wrong sign sample. The Δm^{**} distribution of these events is shown in Figure 6. Excluding the resonance region $0.38 < \Delta m^{**} < 0.44$, nine events are found in the right sign sample, as shown in Fig. 5(b). Figure 7 shows one of the nine events outside the resonance region. In this event, all the particles in the decay with the exception of the neutrino are reconstructed, and the track to vertex assignment is unambiguous.

The signal is estimated from the events with $\Pi > 0.2$, after background subtraction. The number of background events in the signal region is $N_{\mathrm{bkg}} = (f_{\Pi>0.2}/(1 - f_{\Pi>0.2})) \times N_{\mathrm{rsb}}$, where $f_{\Pi>0.2}$ is the fraction of hadronization pions that fall in the signal region, and N_{rsb} is the number of right sign background events in the low probability region. From Monte Carlo simulation, $f_{\Pi>0.2} = 0.100 \pm 0.017$. After subtracting 4.5 events from the low probability region due to signal, $N_{\mathrm{rsb}} = 19.5 \pm 5.0$, and consequently, $N_{\mathrm{bkg}} = 2.2 \pm 0.7$, leaving a signal of 15.8 ± 4.3 events.

The efficiency after requiring $\Pi > 0.2$ is $5.03 \pm 0.85\%$ in the $K^-\pi^+$ channel and $3.42 \pm 0.43\%$ in the $K^-\pi^+\pi^-\pi^+$ channel. The branching ratio for the sum of non-resonant and resonant D_1^0 and D_2^{*0} semileptonic B decays is

$$\mathrm{Br}(b \to \overline{B}) \times \mathrm{Br}(\overline{B} \to D^{*+}\pi^-\ell^-\overline{\nu}X) = (3.7 \pm 1.0_{\mathrm{stat}} \pm 0.7_{\mathrm{syst}}) \times 10^{-3}. \quad (2)$$

4.3 Systematic Uncertainties

Systematic uncertainties which also occur in the measurement of D_1^0 production are estimated as in Section 3.4. The dependence of the fraction of events in the $\Pi > 0.2$ region on various selection criteria for both signal and background has been studied with simulated events, and found to be negligible. In the observed signal it is not possible to disentangle the contribution due to non-resonant $D^{*+}\pi^-$ from the contributions due to wide resonances. These processes are not well known, and could have different efficiencies. In order to allow for these effects, a systematic uncertainty of 10% has been estimated, based on Monte Carlo studies.

The systematic uncertainties are summarized in Table 5.

Source	$\sigma_{syst}(10^{-3})$
B^- Vertex Efficiency	± 0.37
Wide vs. Non-res. Efficiency	± 0.37
Monte Carlo Statistics	± 0.38
D^{*+}, D^0 Branching Ratios	± 0.16
Lepton ID Efficiency	± 0.18
B Fragmentation	± 0.03
B^- Lifetime	± 0.08
Probability Function Π	± 0.12
Total	± 0.72

Table 5: Systematic uncertainties in $\mathrm{Br}(b \to \overline{B}) \times \mathrm{Br}(\overline{B} \to D^{*+}\pi^-\ell^-\overline{\nu}X)$

5 Conclusions

Signals for semileptonic decays of B mesons into both the D_1^0 resonance and into non-resonant $D^{*+}\pi^-$ (or into wide resonances, which are experimentally indistinguishable with this data sample) are observed by the ALEPH experiment at LEP.

The product branching ratio for D_1^0 production is measured to be

$$\mathrm{Br}(b\to\overline{B})\times\mathrm{Br}(\overline{B}\to D_1^0\ell^-\overline{\nu}X)\times\mathrm{Br}(D_1^0\to D^{*+}\pi^-) = (2.04\pm0.58_{\mathrm{stat}}\pm0.34_{\mathrm{syst}})\times10^{-3},$$

From isospin arguments, $\mathrm{Br}(D_1^0\to D^{*+}\pi^-)$ must be less than 2/3. Using the branching ratio $\mathrm{Br}(b\to B^-)=0.37\pm0.03$ from Reference [19], $\mathrm{Br}(\overline{B}\to D_1^0\ell^-\overline{\nu}X)\geq 0.83\pm0.28\%$. Consequently, this mode alone explains at least $20\pm7\%$ of the unidentified semileptonic decays of the B meson.

At the 95% confidence level,

$$\mathrm{Br}(b\to\overline{B})\times\mathrm{Br}(\overline{B}\to D_2^{*0}\ell^-\overline{\nu}X)\times\mathrm{Br}(D_2^{*0}\to D^{*+}\pi^-) \leq 0.81\times10^{-3}.$$

Because $\mathrm{Br}(D_2^{*0}\to D^{*+}\pi^-)$ is 31% or less [9], this does not provide a strong constraint on $\mathrm{Br}(\overline{B}\to D_2^{*0}\ell^-\overline{\nu}X)$.

The product branching ratio for the sum of all decays producing $D^{*+}\pi^-\ell^-\overline{\nu}X$ in the final state is measured to be

$$\mathrm{Br}(b\to\overline{B})\times\mathrm{Br}(\overline{B}\to D^{*+}\pi^-\ell^-\overline{\nu}X) = (3.7\pm1.0_{\mathrm{stat}}\pm0.7_{\mathrm{syst}})\times10^{-3}.$$

If all the $D^{*+}\pi^-$ production is from resonances, either narrow or wide, then the isospin and meson production arguments above give $\mathrm{Br}(\overline{B}\to D^*\pi\ell^-\overline{\nu}X) > (1.5\pm0.5)\%$. These modes thus explain at least $37\pm13\%$ of the unidentified semileptonic decays of the B meson.

Excluding the events close to the D_1^0 resonance, there remain nine events for an estimated background of two events. This is evidence for non-resonant $D^*\pi$ production in semileptonic B decays.

6 Acknowledgements

It is a pleasure to thank our colleagues in the SL division for the successful operation of LEP. We are indebted to the engineers and technicians at CERN and our home institutes for their contributions to ALEPH's success. Those of us not from member states thank CERN for its hospitality.

References

[1] Particle Data Group, Phys. Rev. D 50 (1994) 1173.

[2] M. Voloshin and M. Shifman, Sov. J. Nucl. Phys. 45 (1987) 292.

[3] M. Voloshin and M. Shifman, Sov. J. Nucl. Phys. 47 (1988) 511.

[4] N. Isgur, D. Scora, B. Grinstein, and M. B. Wise, Phys. Rev. D 39 (1989) 799.

[5] E. J. Eichten, C. T. Hill, and C.Quigg, Phys. Rev. Lett. 71 (1993) 4116.

[6] S. Godfrey and R. Kokoski, Phys. Rev. D 43 (1991) 1679.

[7] T. B. Suzuki, T. Ito, S. Sawada, and M. Matsuda, Nagoya University preprint DPNU-93-35, Aichi University preprint AUE-04-93 (1993).

[8] A recent review is M. Neubert, Phys. Reports 245 (1994) 259.

[9] CLEO Collab., P. Avery et al., CLEO preprint CLEO 94-10, CLNS 94/1280.

[10] ALEPH Collab., D. Decamp et al., Nucl. Instr. Meth. A 294 (1990) 121.

[11] G. Batignani et al., IEEE Transactions on Nuclear Science, 39 (1992) 701.

[12] ALEPH Collab., D. Buskulic et al., Phys. Lett. B 313 (1993) 535.

[13] ALEPH Collab., D. Buskulic et al., Phys. Lett. B 295 (1992) 174.

[14] ALEPH Collab., D. Decamp et al., Z. Phys. C 53 (1992) 1.

[15] ALEPH Collab., D. Buskulic et al., Nucl. Instr. Meth. A 346 (1994) 461.

[16] ALEPH Collab., D. Buskulic et al., Phys. Lett. B 307 (1993) 194.

[17] L. Lyons, D. Gibaut, P. Clifford, Nucl. Instr. Meth. A 270 (1988) 110.

[18] ALEPH Collab., D. Buskulic et al., Z. Phys. C 62 (1994) 179.

[19] ALEPH Collab., D. Buskulic et al., Phys. Lett. B 322 (1994) 441.

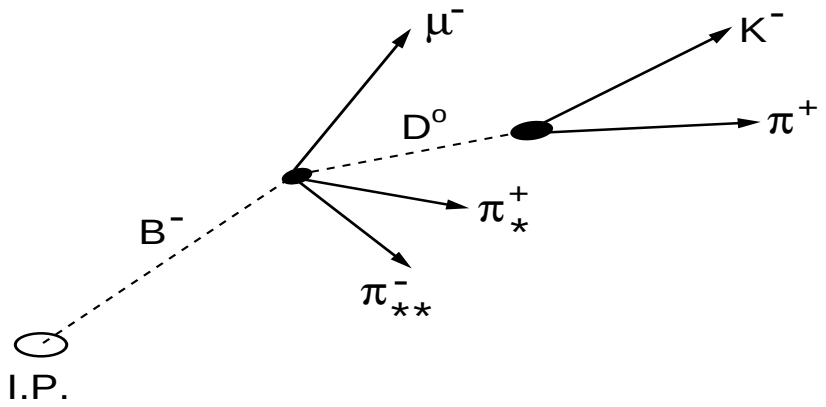

Figure 1: Topology of the decay mode $B^- \rightarrow D_1^0 \mu^- \overline{\nu}$, $D_1^0 \rightarrow D^{*+} \pi_{**}^-$, $D^{*+} \rightarrow D^0 \pi_*^+$, $D^0 \rightarrow K^- \pi^+$.

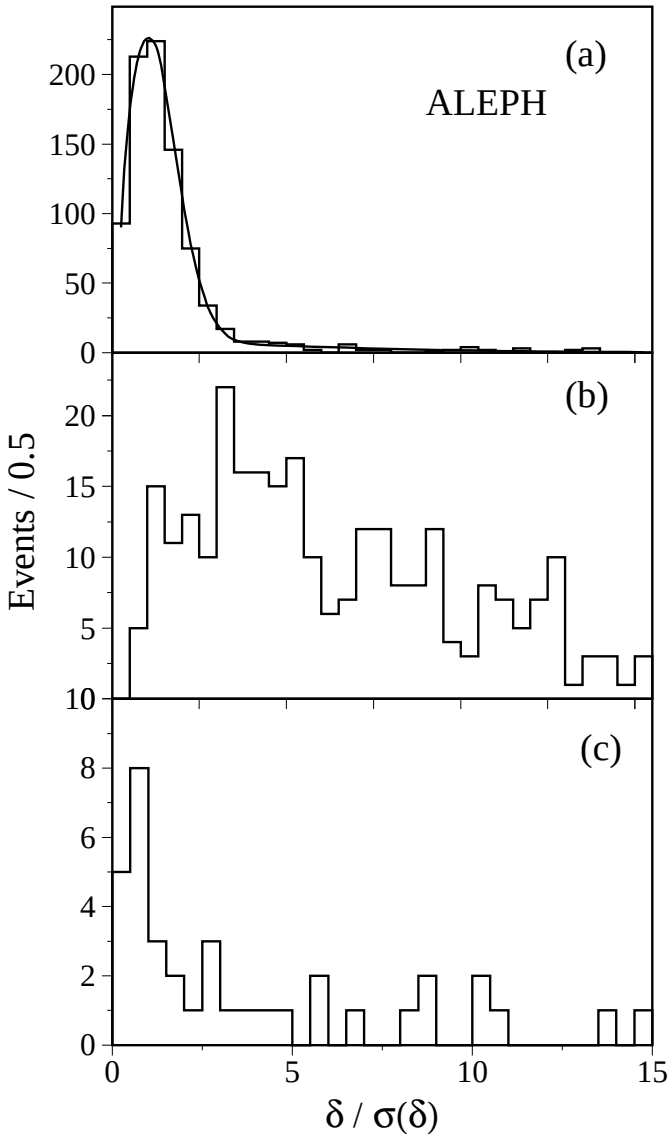

Figure 2: Distance of closest approach of the π^-_{**} to the $D^{*+}\ell^-$ vertex, divided by its error, for (a) the decay $\overline{B} \to D^{*+}\pi^-_{**}\ell^-\overline{\nu}$, from simulation, (b) pions produced in the hadronization of b quarks, from simulation, (c) signal candidates, from data.

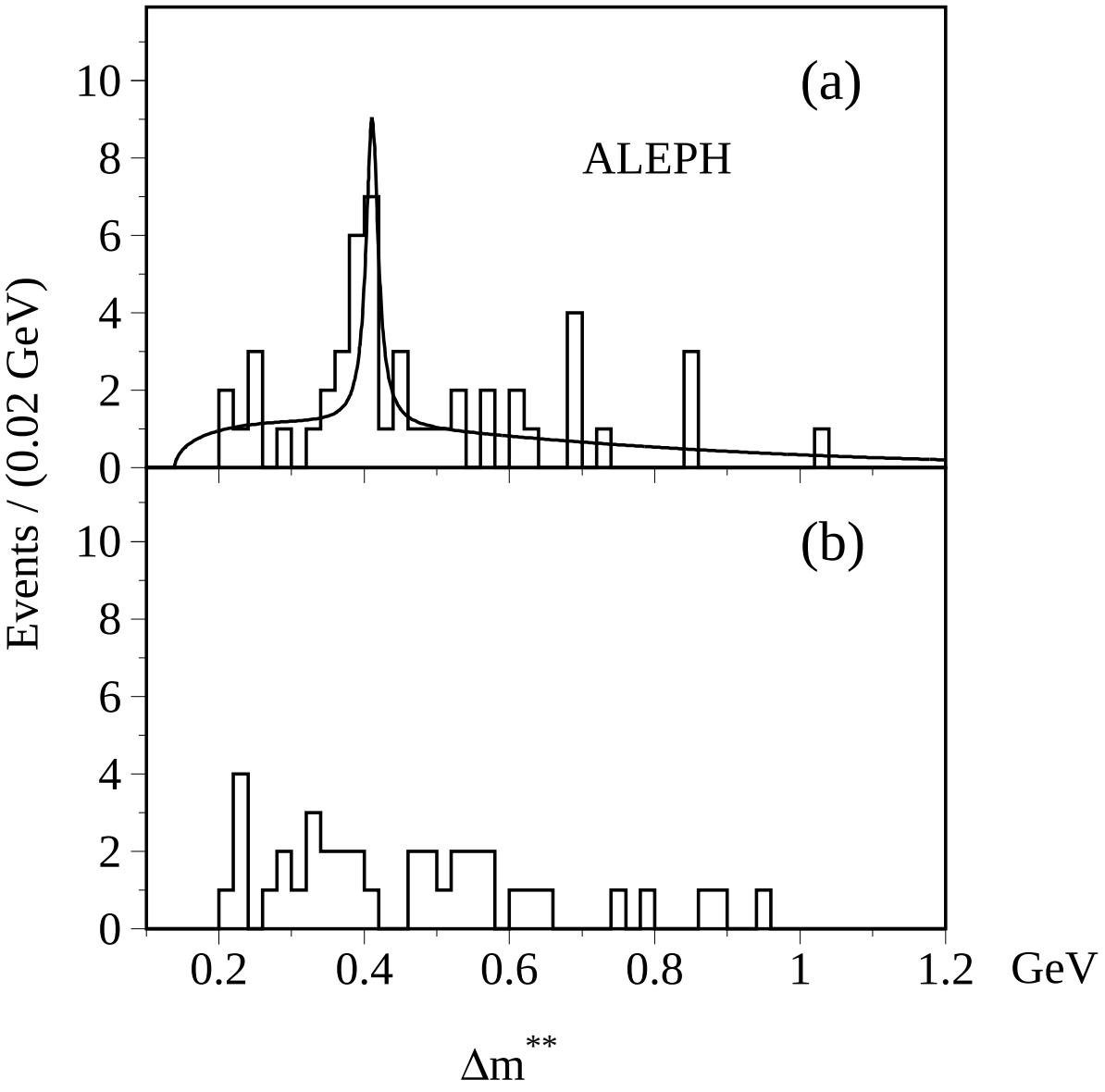

Figure 3: Distribution of Δm^{**}, for (a) the right sign and (b) wrong sign samples, using event selection A. The right sign sample is fitted to a background plus a Breit-Wigner resonance, as described in the text.

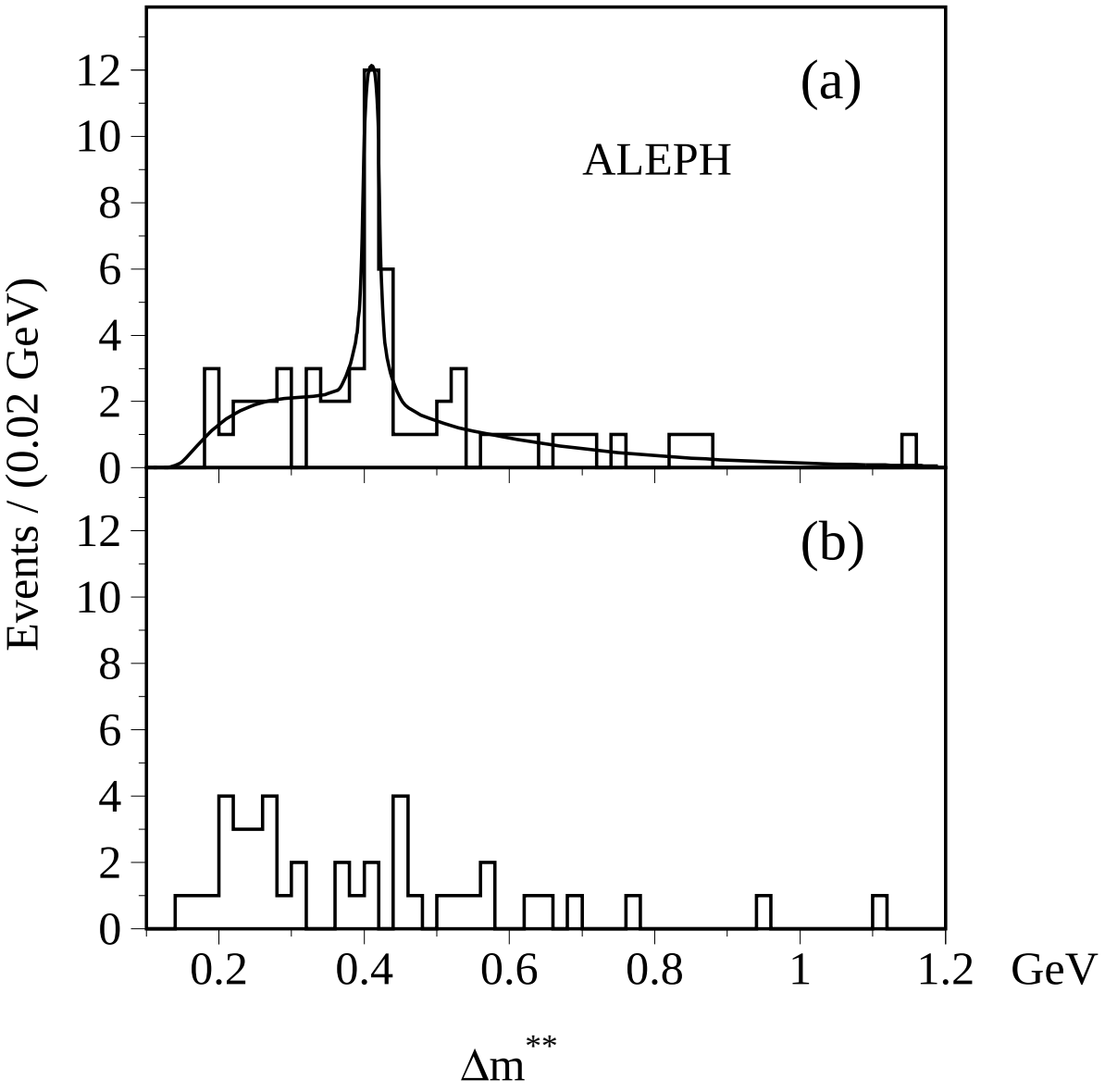

Figure 4: Distribution of Δm^{**}, for (a) the right sign and (b) wrong sign samples, using event selection B. The right sign sample is fitted to a background plus a Breit-Wigner resonance, as described in the text.

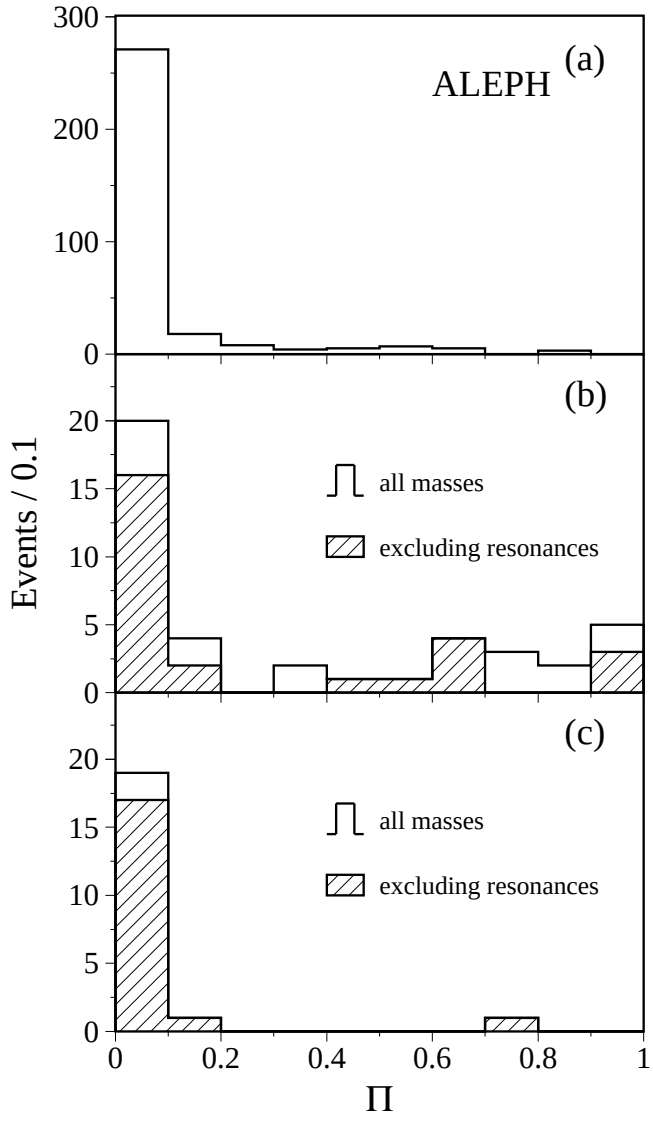

Figure 5: Probability of originating from the $D^{*+}\ell^-$ vertex (Π) for pions in (a) simulated background events, (b) signal candidates in the data, (c) wrong sign pions in the data.

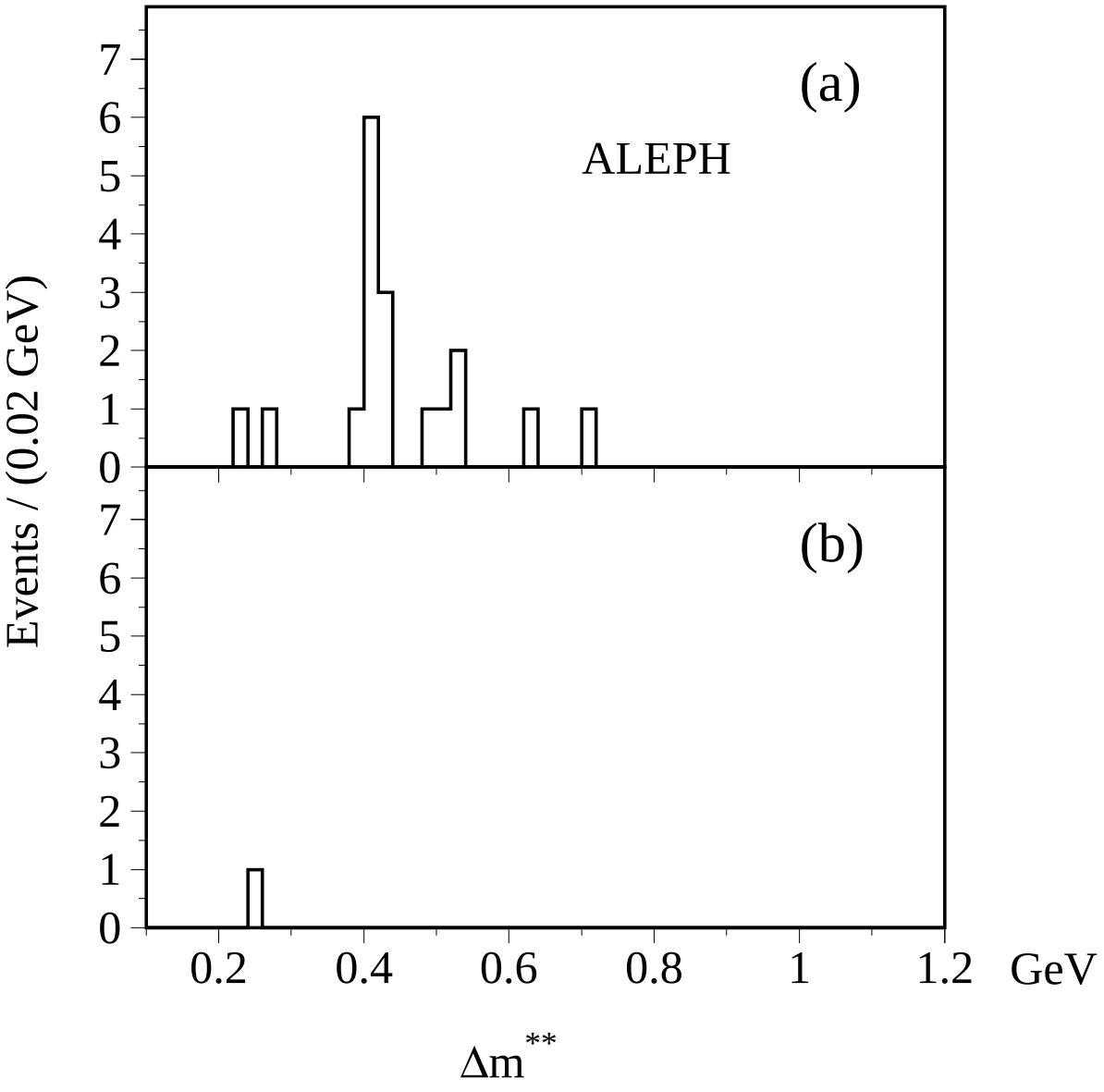

Figure 6: Distribution of Δm^{**}, for (a) the right sign and (b) wrong sign samples, using the event selection of Section 4.1, and with $\Pi > 0.2$.

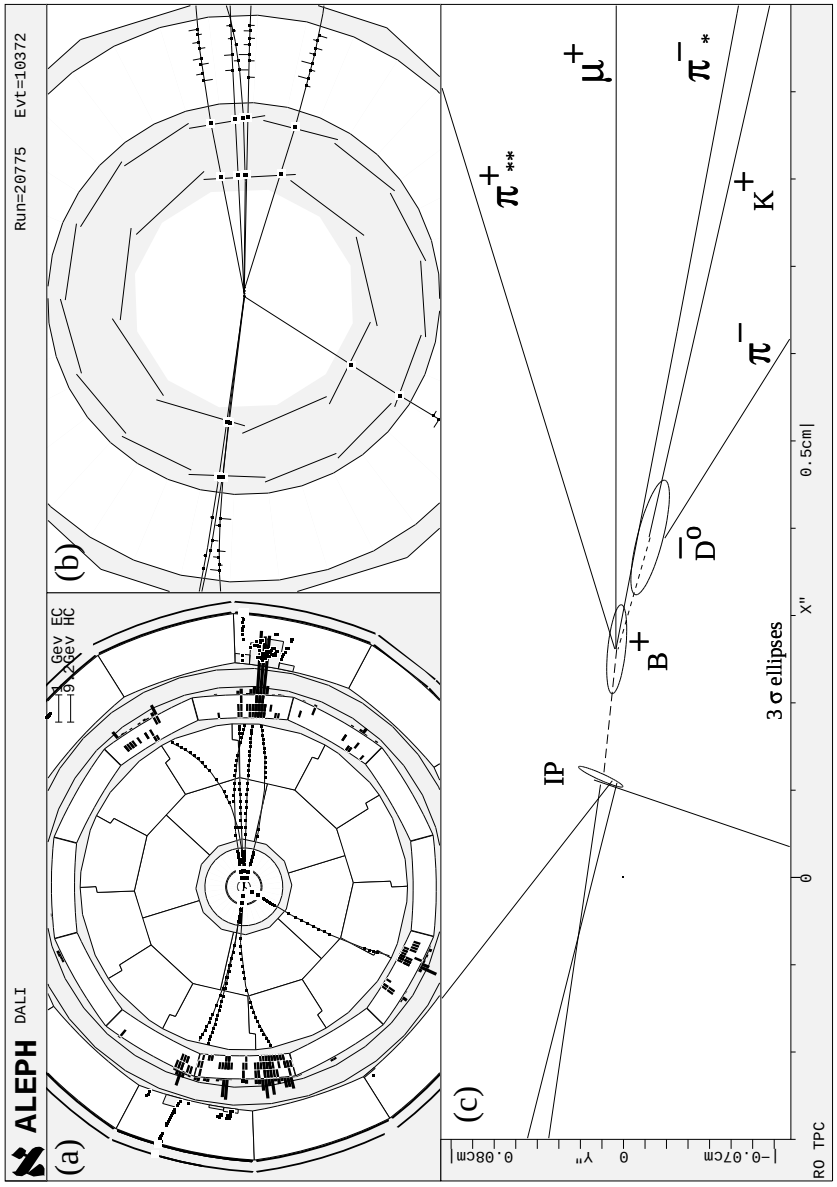

Figure 7: A reconstructed $B^+ \to D^{*-}\pi^+\mu^+\nu$ event. (a) A fisheye $r\phi$ view showing the ALEPH detector. (b) An $r\phi$ view with the VDET and ITC information. (c) A close-up view of the interaction region. The K^+ (identified by its dE/dx) and π^- form a $\overline{D}^0$ vertex with an error of 213 μm along the flight direction. The intersection of the $\overline{D}^0$ flight path with the μ^+ gives the B^+ decay point, which is known to 253 μm along the flight direction. Two pions are unambiguously assigned to this vertex. The negative pion has the low momentum (0.8 GeV/c) characteristic of D^{*-} decay. The 1.9 GeV/c positive pion has a distance of closest approach to the $D^{*-}\mu^+$ vertex is 36 ± 58 μm. The mass of the $D^{*-}\pi^+$ system is 2542 MeV/c^2.